

The role of Coulomb interaction on the electronic properties of monolayer NiX_2 (X = S, Se): A DFT+U+V study

Sergio Bravo,* P.A. Orellana, and L. Rosales

Departamento de Física, Universidad Técnica Federico Santa María,
Av. Espana 1680, Casilla Postal 110V, Valparaíso, Chile

(Dated: August 8, 2023)

The electronic structure of Nickel dichalcogenides, NiS_2 and NiSe_2 , in monolayer form, is studied employing first-principles methods. We assess the importance of band ordering, covalency and Coulomb interactions in the ground state of these systems. Hybrid functional results are compared with standard functionals and also with Hubbard-corrected functionals to systematically address the role of electronic interactions and localization. We found that mean-field correlation realized by intersite Hubbard interactions are directly linked to the magnitude of the energy band gap, giving compelling evidence for the presence of a charge transfer insulating phase in these materials.

I. INTRODUCTION

Two-dimensional (2D) Van der Waals materials have emerged as a class of systems that have proven to hold great potential for realizing new physics as well as novel technological capabilities. One of the sets that has aroused a high level of interest in recent times are the transition metal dichalcogenides (TMD). They exhibit an attractive combination of atomic-scale thickness, strong spin-orbit coupling, direct bandgap, and favorable electronic and mechanical properties [1]. This makes them interesting for basic research and for example, high-end electronics and spintronics applications.

Even with these advances, there remain many 2D TMD that deserve to be investigated in more detail. To this category belong the Nickel dichalcogenides NiX_2 , with X=S, Se, Te. This group of materials has been proposed theoretically [2, 3] in the 2H and 1T phases and also realized experimentally, in the case of 1T NiSe_2 [4]. The properties studied are related to band engineering [5], thermoelectric efficiency [6], anode materials in batteries and also superconductivity [7]. One of the ingredients that is lacking in these recent studies is the inclusion of electronic interactions. As we know, the presence of localized d orbitals in transition metals make necessary that the correlation effects are accounted for so that the predicted physical properties are closer to reality. The level of refinement in the treatment of interactions varies widely, and factors that impact the selection of a method stems from the size of the system, the type of the components and the available computational resources. Examples of methods that treat the interacting problem are the Hartree-Fock approximation [8], GW approximation [9], mean-field approximations [10], density functional theory [11], dynamical mean-field theory [9] and coupled cluster theory [12], which form just a limited list. Among the possible methods mentioned, mean-field methods along with density functional theory (DFT), are the fastest and most flexible in computational terms. This allows to

study systems with considerable sizes and different kinds of structure without high cost. Inside the DFT framework, one of the implementations of electronic interactions at the mean-field level that is widely used, is known as Hubbard-corrected DFT, or DFT+U, for its early implementation [13, 14]. This formalism adds a minimal term to the original DFT energy functional which accounts for onsite Coulomb repulsion (U) at the atoms with localized orbitals[14]. This approach has been very successful, and in recent years, it has been implemented in extended form by including not only onsite parameters but also intersite interactions [15–17]. This last method is starting to be used in studies of different materials [18–23], giving new perspectives on the incidence of interactions on the electronic structure.

To study the effects of correlation in NiX_2 systems, in this work, we employ DFT with Hubbard corrections and also with hybrid functionals in order to characterize NiS_2 and NiSe_2 in the 1T monolayer form. We carry out a band structure study in momentum space along with real space orbital characterization to explore the role of Coulomb interaction in these systems at the mean-field level. Complementary, a charge transfer phase is identified in both materials, and its origin is discussed.

The manuscript is organized as follows. First, we detail the computational resources and corresponding settings for the first-principles calculations. Next, we mention the more salient structural properties of NiX_2 . The calculations using the non-corrected DFT methods are presented in section III B along with the results of the electronic structure using a hybrid functional. Also, we present a discussion of the basic electronic features. This is followed in III C by the main calculation of the work. Namely, the application of the Hubbard-corrected DFT method, which is accompanied by the self-consistent calculation of the Hubbard parameters by a linear response approach. Comparison of this last procedure with the hybrid functional outcome is addressed and in section III D a possible route to improve the Hubbard-corrected results is developed. We conclude the article by exposing final remarks and giving an outlook for future work. Additional data and figures that complement the results

* sergio.bravoc@usm.cl

and discussion presented in the main text has been left as supplementary material (SM).

II. COMPUTATIONAL DETAILS

All calculations were carried out using the QUANTUM ESPRESSO package (QE) [24]. We use three types of functionals. Namely, the standard GGA-PBE functional, a modified PBE functional with Hubbard corrections (also called DFT+U+V) according to implementations in [15] and the hybrid HSE06 (HSE) functional [25] with the ACE implementation [26]. Relaxed structures were obtained at PBE and DFT+U+V levels with a force tolerance of 10^{-2} eV/Å per atom and an energy tolerance of 10^{-8} Ry. A vacuum layer of 20 Å was used to simulate the layered character of the systems. The energy cutoff for the self-consistent calculations was set to 100 Ry for all cases with a tolerance of 10^{-8} Ry. Calculations included the possibility of magnetic final states without considering spin-orbit coupling, that is, a spin-polarized setting. The k -space Monkhorst-Pack grid was fixed to $15 \times 15 \times 1$ points for all calculations. In the case of HSE functional, the Fock operator was calculated with a q-space grid of $5 \times 5 \times 1$ points.

For the linear response calculations that allow the self-consistent computation of the Hubbard parameters, the HP code was used [27], as part of the QE suite. The code requires a self-consistent ground state calculation of QE as starting point. We use the ortho-atomic type of projectors for this calculation, which sets the basis for the occupations matrices (see section III C) with Löwdin orthogonalized atomic orbitals. Well-converged results for the values of the parameters were obtained using a q-space grid with $5 \times 5 \times 1$ points and a tolerance of 10^{-7} eV for the response function χ , defined in [27].

III. RESULTS

A. Structural properties

Nickel chalcogenides NiX_2 in 1T phase can crystallize in monolayer form with a trigonal lattice structure, as shown in Fig. 1a. The transition metal is located at the corners of the unit cell forming a triangular sub-lattice while the chalcogen atoms form a buckled hexagonal sub-lattice. This structure is described by space group (SG) $P\bar{3}m1$ (#164) [28]. This symmorphic SG has 12 symmetries generated by spatial inversion I , a three-fold rotation about an axis perpendicular to the monolayer plane, and a two-fold rotation about an axis that is in the monolayer plane along the lattice vector $\mathbf{a}_1 + \mathbf{a}_2$ (see Fig. 1a for the lattice vectors representation). The relaxed structure obtained from our calculations gives that a generic Ni atom is six-fold coordinated, and the NiX_6 subsystem forms a distorted octahedron. Thus, for instance,

using NiSe_2 , we obtained that the elongated Se-Ni-Se angle has a magnitude of 95.58° , departing from the ideal right angle. Additional data concerning lattice parameters and bond lengths arising from the first-principles calculations detailed below, are presented in the SM. The values reported in this work agree well with previous studies [3, 4, 7].

One important consequence of the atomic landscape is that Ni atoms experience the well-known crystal field splitting associated to the interaction with chalcogen orbitals. This splitting can be directly deduced from the SG information by taking into account that the atom located at the unit cell corner (1a Wyckoff position to be more precise [29]), have a site symmetry isomorphic to point group (PG) $3m1$. The dimensionality of the irreducible representations of this PG gives the maximal degeneracy that a set of orbitals can have. Using the tabulated information from the Bilbao Crystallographic Server [30] we can see that the greatest degeneracy that orbitals can have in this the atomic environment is two. If we take into account the basis of atomic orbitals, we can see that, for example, d -orbitals will split into three sets; one nondegenerate orbital and two sets of orbitals each with a double degeneracy. The presence of these two-fold degenerated orbitals will induce two-fold degeneracies in momentum space. This real space momentum space relation will dictate the general form that the electronic structure will show in what follows.

B. Orbital order and first electronic structure description

Although correlated systems could be studied by more elaborated methods [9], we take here a mean-field approach, as this can serve as a baseline for understanding the incidence of interactions in these TMD. The standard starting point of this approach is to perform an electronic structure at the level of the generalized gradient approximation (GGA) with the PBE functional. In the following, we present results for the NiSe_2 monolayer and refer the reader to the SM for analogous figures and data concerning the NiS_2 monolayer. In first place, we present the NiSe_2 electronic band structure in Fig. 2b. The plot also contains information about the orbital projection along the high-symmetry path delimited by the high-symmetry points (HSP) in the Brillouin zone (BZ), as represented in Fig. 1b. The PBE projected bands show a clear tendency even at this level; upper valence bands show a clear p -orbital type coming from Se atoms. However, deep valence bands have a more mixed character, they are formed by the strong hybridization of Ni d -orbitals and Se p -orbitals, as expected by the features of the lattice structure. This orbital energy order is similar to the behavior observed in charge-transfer insulators [31]. Specifically, when the p orbitals are on top of the d orbitals in the valence bands, the material will present a small or even negative charge-transfer gap [31]. This

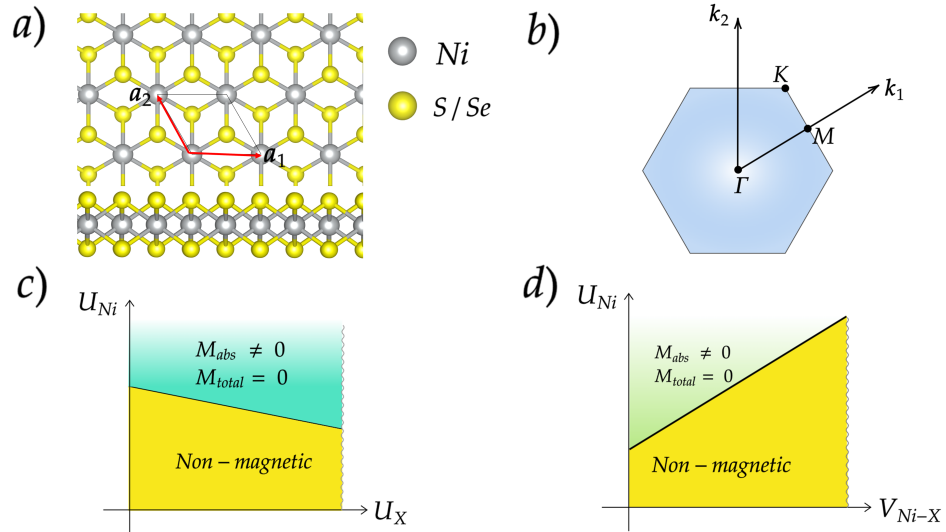


FIG. 1. a) The lattice structure of monolayer NiX_2 . b) Two-dimensional Brillouin zone for the monolayer NiX_2 systems. c) Magnetic phase diagram for U_{Ni} versus U_S for fixed intersite interaction V_{ij} . The range of values for U_{Ni} was from 0 eV to 9 eV. For U_X was from 0 to 4 eV. d) Magnetic phase diagram for U_{Ni} versus V_{NiX} for fixed onsite interaction U_X . The range of values for U_{Ni} was from 0 eV to 9 eV and V_{NiX} was from 0 to 3 eV.

charge transfer can be understood as the passing of electronic charge from the p -shell at chalcogen atoms to the d -shell belonging to the transition metal. This is formally represented as $d^n p^6 \rightarrow d^{n+1} p^5$ and in this type of systems, this process will correspond to the low-energy excitations [32]. However, as it is well-known, PBE results consistently underestimate localization effects and systematically tends to delocalize electrons [11] which results in a sometimes deficient prediction of the ground state properties. For transition metal compounds, this is a well-documented issue and methods to improve the PBE results are needed to meet experiments [14]. Following this line, we will explore two levels of extension of the PBE results. In this section, we present the first one. In Fig. 2a, the electronic band structure resulting from using a hybrid HSE functional is shown. This functional, by definition, includes a part of the exact exchange [25]. The hybrid band structure exhibits a gap of approximately 1 eV, which, as expected, is greater than the PBE band gap, which has a magnitude of ~ 0.6 eV. Another difference stems from the dispersion of top valence bands and their interaction with deep valence bands. It can be observed that the HSE result yields a more clear separation between the set of upper and lower valence bands and higher dispersion for the upper valence bands. These effects can be traced to including localization in the hybrid case. This can be observed if we study the real space orbital character of NiSe_2 , using the local density of states. More in detail, in Fig 3 we compare the level of localization for the low energy range of the system obtained from the hybrid functional versus the PBE result, represented by the integrated local density of states (ILDOS). Although the results coincide

roughly, a closer look show that the p -orbitals contribution to the conduction bands is more localized in the HSE case (Fig 3a top) with respect to the PBE result (Fig. 3b top). Also, for the upper valence bands, states situated at Ni atoms show a slightly more delocalized appearance in PBE (Fig. 3b lower panel) in comparison with the HSE case (Fig. 3a, lower panel). All the above discussion indicates that the inclusion of electron correlations in monolayer NiX_2 materials should play a key role to describe properties derived from the electronic structure. In principle, we can stay with the hybrid functional as the final result. However, hybrid functionals suffer from technical complications related to the computational effort to calculate the exact exchange and this fact hinders their utilization in wider applications. Also this kind of functionals also lack other contributions to correlation [9] and thus more sophisticated approaches should be used, such as GW calculations and dynamical mean-field methods. Despite of this, the HSE result represents a significant improvement over the bare PBE calculation. Thus, in the following, we take the HSE ground state as a reference and compare it with another method that tries to improve on the PBE level by including Coulomb interactions at the mean-field level.

C. DFT+U+V approach and linear response calculations

We have calculated the electronic structure of NiX_2 materials considering the inclusion of correlation through Hubbard parameters. We introduce the parameters by resorting to a simplified model to visualize this setting better. From the above calculations, we can identify the

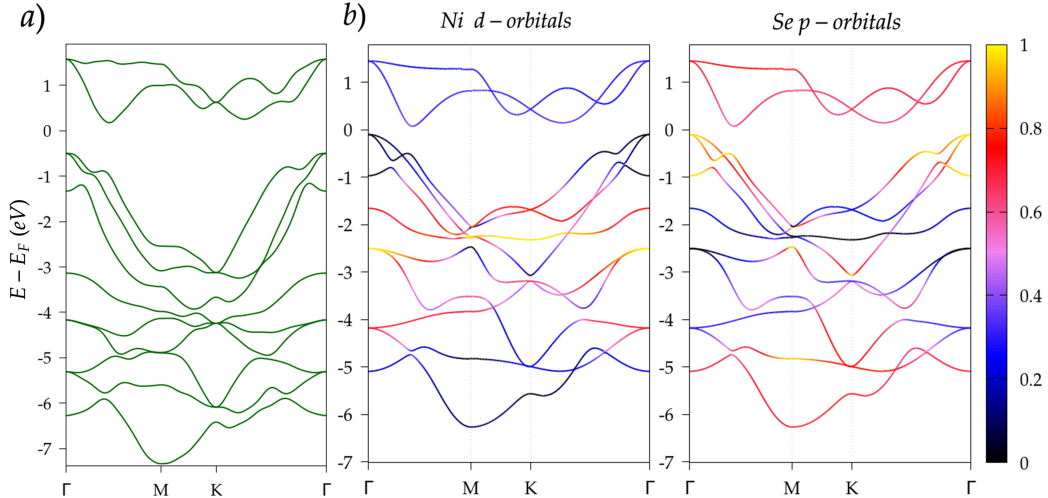


FIG. 2. a) HSE electronic band structure for NiSe₂. b) PBE electronic band structure with orbital projections for (left) Ni *d*-orbitals and (right) Se *p*-orbitals. The color scale at the right is in states · Å²/eV units.

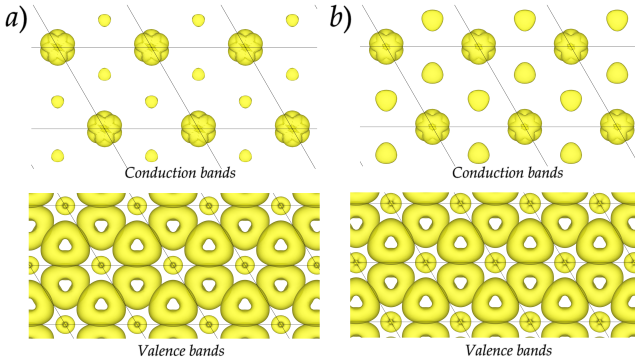


FIG. 3. a) Integrated local density of states for (top panel) lowest conduction bands and (bottom panel) top of the valence bands with the HSE functional for NiSe₂. b) Integrated local density of states for (top panel) lowest conduction bands and (bottom panel) top of the valence bands with the PBE functional for NiSe₂. In both cases, the valence band range is 0.4 eV from the top of the bands. The conduction band integration range goes from Fermi level to 1.5 eV.

Ni *d*-orbitals and the Se (S) *p*-orbitals as the most important orbitals. Using a tight-binding representation with no correlation, the low energy Hamiltonian takes the following form

$$H_0 = \epsilon_d \sum_{\alpha} d_{\alpha}^{\dagger} d_{\alpha} + \epsilon_p \sum_{\beta} p_{\beta}^{\dagger} p_{\beta} + \sum_{\alpha\beta} t_{\alpha\beta} (d_{\alpha}^{\dagger} p_{\beta} + \text{h.c.}) . \quad (1)$$

Here d_{α}^{\dagger} and p_{β}^{\dagger} are the creation operators for an elec-

tron in *d*-orbitals and *p*-orbitals, respectively. The terms in the first line correspond to onsite energies and the last term is the hopping parameter that serves to implement hybridization among Ni and Se orbitals. The inclusion of correlation is realized as an extended Hubbard model that is expressed as [31]

$$H_{UV} = H_0 + U_{Ni} \sum_{\alpha} n_{d_{\alpha}} n_{d_{\alpha}} + U_X \sum_{\beta} n_{p_{\beta}} n_{p_{\beta}} + V_{NiX} \sum_{\alpha\beta} n_{d_{\alpha}} n_{p_{\beta}} + V_{XX} \sum_{\gamma} n_{p_{\beta}} n_{p_{\gamma}}, \quad (2)$$

where $X = S, Se$.

In this Hamiltonian, $n_{d_{\alpha}}$ and $n_{p_{\beta}}$ denote the occupation operators for *d* and *p* orbitals, respectively. The second and third terms represent the so-called onsite Hubbard parameters that quantify the cost in energy of double occupancy for a *d*-orbital (U_{Ni}) and a *p*-orbital (U_X). The fourth term, with coefficient V_{NiX} , represents an extension of the theory to include the intersite interaction between occupations among the *d* and *p*-orbitals. The last term is also an intersite interaction between the next-nearest neighbors of the Se-Se type in this class of materials. In practice, we include two of these (Se-Se) interactions; second and third neighbors. We stop at this level and leave more distant correlations outside the subsequent calculations.

A density functional theory implementation of the interactions presented above, with a self-consistent and rotational invariant character is employed for the calculation of the ground states. This level of theory is customarily denoted as DFT+U+V [15]. We do not enter into the details of the theory here as this has been extensively

exposed in recent works [18, 19]. We only mention that the formalism is based on the modification of the original DFT framework by the addition of a correction term $E_{U,V}$ giving a new energy functional $E = E_{DFT} + E_{U,v}$. The key ingredients of the $E_{U,V}$ term are the so-called occupation matrices $n_{m,m'}^{IJ\sigma}$ which are defined by the projection of the Kohn-Sham eigenfunctions ψ_μ^σ (σ labels spin) on a set of localized orbitals ϕ_m^I (J labels the atomic site and m labels the orbital quantum number), such that [14]

$$n_{m,m'}^{IJ\sigma} = \sum_\mu f_\mu^\sigma \langle \psi_\mu^\sigma | \phi_{m'}^J \rangle \langle \phi_m^I | \psi_\mu^\sigma \rangle. \quad (3)$$

The coefficients accompanying these matrices are the Hubbard onsite and intersite parameters presented above. The $n_{m,m'}^{IJ\sigma}$ are obtained in a self-consistently way along the energy computation and comprise an appropriate model for interactions at the mean-field level, with the advantage of being part of a fast and flexible framework.

As has been made patent by the model presented, the Hubbard parameters will modify the localization character of the orbital manifolds of interest. However, until recently, the most used procedure was to set the parameters in a semi-empirical way, resorting to experimental references or previous numerical benchmarks [33]. Presently, the approach is to calculate these parameters in a self-consistent manner and various alternatives have been made available [16, 17, 34].

For this work, we use the DFT+U+V approach as formulated in [35]. The Hubbard parameters are computed within this framework using density functional perturbation theory, also known as a linear response (LR) calculation. Section II presents the specific settings used for the calculations in this work. We now outline the procedure that has been put forward for procuring a converged set of parameters. In the first place, the calculation needs an initial guess for the Hubbard parameters. We have started from zero values and, with this set, run a first calculation. One of the subtle points is that our starting configuration concerns an insulating phase with no magnetic state. However, as it is well-known, variations of the electron interaction strength could result in magnetic states and also in metal-insulator transitions [31]. Thereby, after the initial LR computation (first shot), we carried a new ground state computation with the obtained set of parameters. This calculation shows that the actual ground state is metallic and magnetic at this point of the process. The material also suffers from an enlargement of the unit cell due to the increment of the interactions (See the SM for a summary of the geometric parameters obtained for the magnetic phases). We therefore, go to obtain new relaxed coordinates. This ground state is now used as the input of a second shot for the LR calculation to see how parameters vary. After this shot, the procedure explained after the first shot is repeated until the magnitude of the parameters does not change

above a desired tolerance. For our purposes, we set the threshold at 0.1 eV, where we noted that the electronic structure does not suffer appreciable changes for all the considered parameters. This iterative process yields the LR Hubbard parameters that are presented in TABLE I. The final phase obtained from LR is a magnetic metallic state. In particular, we find a compensated ferrimagnetic (FiM) ground state, which has a zero total magnetization and a nonzero absolute magnetization of $\sim 2.7 \mu_B/\text{cell}$ for NiS_2 and $\sim 3.1 \mu_B/\text{cell}$ for NiSe_2 . The microscopic magnetic ordering that is realized entails an antiferromagnetic (AFM) interaction among the Ni atoms and the chalcogen atoms. This AFM coupling is complemented with a complete compensation of magnetic moments in the unit cell, resulting in zero total magnetization. The electronic band structure that is obtained for this phase is presented in the SM.

In view that a double transition has occurred in the system, we decided to carry out a study of the magnetic properties of the system. We achieve this through performing several DFT+U+V calculations within a range of values for U and V parameters (See caption of Fig. 1a and b). To achieve this, we conduct multiple DFT+U+V calculations using different values for the U and V parameters (as indicated in the caption of Fig. 1a and b). Observation of the trends in these calculations indicates that the FiM state is very robust, as it is the only ground state encountered for the range of values explored (without considering eventual lattice distortions that could change the space group symmetry). This FiM state appears even in the case where only U_{Ni} is nonzero. Considering the former and the tendency to an AFM coupling, we can expect that the final FiM state will be produced due to the difference in localization of the p electrons in comparison with d electrons; the more itinerant p electrons tend to metalize the system, while d electrons will tend to stay localized. In the overall, for a sufficiently high U_{Ni} interaction (of the order of ~ 6.5 eV for both materials), it will be favorable to produce a conducting channel with only one type of spin polarization, leaving the remaining channel insulating. Therefore in comparison with our reference calculation, the hybrid functional result of section III B, the LR is not giving the correct ground state. Nevertheless, the inspection of the magnetic phase diagrams points to the fact that the state similar to the reference calculation must be located in the nonmagnetic zone but with nonzero interaction parameters. If the resulting values of the LR calculation are considered and compared with values extensively used [36, 37], it can be concluded that the actual magnitude of the onsite Hubbard parameters, U_{Ni} and U_X are in good agreement with previous works. This is not the case for the intersite parameters, due to the scarce availability of results. Thus in the next, we will explore the implications of keeping onsite values fixed while varying the intersite parameters. A guideline that this is indeed plausible is that, observing the U_{Ni} versus V_{NiX} diagram in Fig. 1d, if we start in the FiM region and move horizontally in the graph to greater values

Material	U_{Ni}	U_X	V_{NiX}	$V_{XX}^{(1)}$	$V_{XX}^{(2)}$	\bar{V}_{NiX}
NiS_2	6.79	3.84	0.68	0.51	0.47	1.8
NiSe_2	6.5	3.53	0.61	0.45	0.41	2.3

TABLE I. Hubbard parameters obtained from linear response calculations for monolayer NiS_2 and NiSe_2 . The last column reports the modified values used for the first neighbor intersite interactions. All values are in eV units.

of V_{NiX} , we end invariably in a nonmagnetic correlated state.

D. Control of the energy gap by minimal modification of the linear response result

As mentioned in the previous section, we will examine how to modify the results from LR to attain a more similar state to that of our reference hybrid functional. The idea, the basis of which was established above, is only to alter the inter-site parameters. This is in the spirit of minimizing the arbitrary adjustments in the study. To constrain even more the approach, we mention that, from the calculations mentioned in the previous section, the V_{XX} interactions do not have a substantial impact on magnetic properties of the systems. Therefore, we propose a minimal modification that will consist of to only change the V_{NiX} parameter, the other parameters remaining at the same values as in the original LR calculation. We have increased V_{NiX} beyond values where a magnetic phase transition is produced, implying a metal-insulator transition. Both transitions happen at almost the same V_{NiX} values. The trend observed in the process is that the absolute magnetization decreases when V_{NiX} grows. This happens up to a point where it abruptly goes to zero. The critical value found was $\sim 1.6\text{eV}$ for NiS_2 and $\sim 1.8\text{eV}$ for NiSe_2 . This magnetic transition is also accompanied by a reduction of the lattice parameter of the unit cell in such a way that, after the transition, the system recovers the original lattice constant found in the non-interacting GGA calculation.

As a result, the system will no longer have magnetic properties and will display an energy gap beyond this point. At this stage, the most notable aspect is that as the parameter increases, there is an increase in the energy gap of the system. In simpler terms, there is a direct relationship between the value of V_{NiX} and the size of the gap. To compare with the hybrid case, our criterion for setting the value of V_{NiX} is to match the energy gap magnitude obtained from the HSE calculation. We present the values that meet this requirement in TABLE I. With these values plus the rest of the LR parameters, we perform a band structure calculation. Results are plotted in Fig. 4a, along with a ILDOS calculation, shown in Fig. 4b. It can be recognized right away that the inclusion of correlation gives a more localized character to the states for both Ni d orbitals and Se p orbitals (A similar cal-

culation for NiS_2 is available in the SM). This is what is expected from previous results. Also, the dispersion of top valence bands becomes very similar to the hybrid bands in Fig. 2a.

The band gap dependence on V_{NiX} can be linked to the charge transfer properties of the materials. As has been discussed previously, without Hubbard corrections, the system already show an inverted valence band ordering similar to the case of transition metal oxides [31]. At this PBE level, if final orbital manifold occupations are computed, it is obtained that, for Ni atoms, there exists a considerable outer shell occupation of ~ 9.20 . Formally, Ni must be in a state with d^6 . On the other hand, the p -shell of each Se (S) atom finishes with an occupation of 4.40. Formally, the initial state of this manifold is p^6 . Thus we have evidence that a charge transfer has occurred, where the p -shell occupation of each chalcogen atom has changed by approximately 1.5. This implies a p -hole formation, a well-known phenomenon in these charge transfer systems [32]. The inclusion of correlations alters occupations slightly. But the tendency gives us clues about the behavior of the electronic structure. Thus, if we start from the LR original state (no parameter modification), the occupation of the Ni d shell decreases and increases for the Se (S) p -shell. This is understandable because the rise in electronic localization hinders charge transfer. However, the system remains in the charge transfer regime as p orbitals continue to be higher in energy with respect to d orbitals. Now when V_{NiX} departs from the LR result to higher values, if the state is still in the FiM state, the charge transfer process shows an opposite pattern of evolution for different atoms and spins. That is to say, for the chalcogen atoms, the majority spin gets its occupations diminished while the minority achieves greater occupations. In the case of the Ni atoms, the behavior gets reversed. This mechanism conflates so that the spin unbalance is utterly canceled. Once inside the non-magnetic phase, the augmentation of V_{NiX} has the effect of reducing the charge transfer. This reduction is coupled with a new increase in localization, which competes with the orbital mixing between Ni and Se (S) atoms. The former is traduced in energy level repulsion. This implies that bonding d orbitals will get deeper in energy, separating from the bands with a predominantly p -type character. Thus, the corresponding antibonding orbitals associated with the lower conduction bands will increase their energy. Overall, the band gap grows, controlled by the value of the intersite interaction. In other words, the increase of V_{NiX} will make energetically more costly the generation of charge transfer excitations, which traduces in a greater band gap.

IV. DISCUSSION AND CONCLUDING REMARKS

To put in perspective the findings obtained, we can make a few additional remarks. First, although the

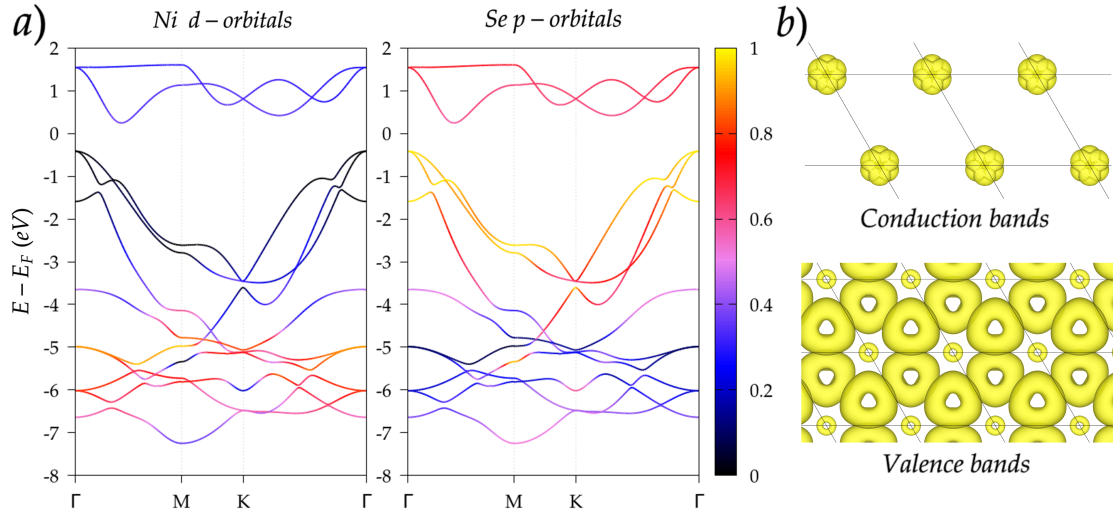


FIG. 4. a) Orbital-projected electronic band structure at the DFT+U+V level of NiSe₂ with parameters from linear response with modified V_{NiX} parameter. The color scale at the right is in $(\text{states} \cdot \text{\AA}^2)/\text{eV}$ units. b) Integrated local density of states for (top panel) lowest conduction bands and (bottom panel) top of the valence bands using the DFT+U+V functional with linear response parameters with modified V_{NiX} .

PBE level already shows the distinctive indicators of the charge transfer state, such as the inverted band ordering, correlations must be included in this type of system since it is a crucial competing mechanism for covalency and orbital hybridization. As shown above, it is a correlation that defines the magnitude of the energy band gap, which is important, for example, to study optical responses. Regarding the LR calculation, although this phase does not seem to be the one that experimentally materializes [4], we found that the calculation is useful to get an idea of the order of magnitude of the parameters that the systems could have. Also, considering the technical part, we have tried to amend the outcome by starting from different insulating and metallic states, and ultimately the calculation consistently tends to the featured magnetic phase. This could be linked to an already recognized issue related to calculations on systems with a nearly full shell [27, 35]. Despite that, the minimal modification presented here is a valuable prospect for performing future physical response computations involving electronic correlation. Viewing the entire array of results, if the insulating phase is corroborated in subsequent studies, the charge transfer phase will be an interesting system to analyze further. This is because, as has been identified in other works, the *p*-hole formation, also known as self-doping, could lead to other effects when the system is perturbed [31, 32, 38, 39]. The interplay between the two-dimensional character of the materials and this *p* orbital dominance could also lead to novel phenomena.

In summary, we have put forward a detailed analysis

of the electronic structure of monolayer transition metal dichalcogenides, NiS₂ and NiSe₂ using a variety of first-principles methods. This allows us to ponder the role that electronic interaction plays at the mean-field level. An hybrid HSE functional was used as the first reference in regard that the inclusion of correlations is built-in in its formulation. Comparison with modern Hubbard corrected PBE functionals allowed a further understanding of the importance of localization and the relation to the charge transfer effect. We demonstrate that nearest-neighbor intersite parameter V_{NiS} is directly linked to the energy band gap of the ground state, as this parameters control the Ni-X hybridization and the charge transfer excitations. In the future, further analysis of this problem will focus on enhancing the inclusion of correlation through more advanced calculations, such as GW calculations. Investigating how the DFT+U+V method measures up against other state-of-the-art approaches would be quite intriguing. Ultimately, our goal is to highlight the importance of including more interaction parameters in studies like this. Doing so could offer new insights into the behavior of correlated systems.

ACKNOWLEDGEMENTS

This work has been supported by the Postdoctoral Grant from Universidad Técnica Federico Santa María, and Chilean FONDECYT Grant 1220700.

[1] S. Manzeli, D. Ovchinnikov, D. Pasquier, O. V. Yazyev, and A. Kis, 2D transition metal dichalcogenides, *Nature Reviews Materials* **2**, 17033 (2017).

[2] J. Zhou, L. Shen, M. D. Costa, K. A. Persson, S. P. Ong, P. Huck, Y. Lu, X. Ma, Y. Chen, H. Tang, and Y. P. Feng, 2dmatpedia, an open computational database of two-dimensional materials from top-down and bottom-up approaches, *Scientific Data* **6**, 86 (2019).

[3] M. N. Gjerding, A. Taghizadeh, A. Rasmussen, S. Ali, F. Bertoldo, T. Deilmann, N. R. Knøsgaard, M. Kruse, A. H. Larsen, S. Manti, T. G. Pedersen, U. Petralanda, T. Skovhus, M. K. Svendsen, J. J. Mortensen, T. Olsen, and K. S. Thygesen, Recent progress of the computational 2d materials database (c2db), *2D Materials* **8**, 044002 (2021).

[4] Y. Shao, S. Song, X. Wu, J. Qi, H. Lu, C. Liu, S. Zhu, Z. Liu, J. Wang, D. Shi, S. Du, Y. Wang, and H.-J. Gao, Epitaxial fabrication of two-dimensional NiSe₂ on Ni(111) substrate, *Applied Physics Letters* **111**, 10.1063/1.4991065 (2017), 113107.

[5] H. Khalatbari, S. I. Vishkayi, M. Oskouian, and H. R. Soleimani, Band structure engineering of nis₂ monolayer by transition metal doping, *Scientific Reports* **11**, 5779 (2021).

[6] Anisha, R. Kumar, S. Srivastava, and K. Tankeshwar, Optimising 1t-nis₂ monolayer thermoelectric performance via valley engineering, *Materials Today Communications* **34**, 105169 (2023).

[7] R. Ku, L. Yan, K. Xue, J. Zhang, K. Pang, M. Sha, B.-T. Wang, Y. Jiang, L. Zhou, and W. Li, Nix₂ (x = s, se, and te) monolayers: Promising anodes in li/na-ion batteries and superconductors, *The Journal of Physical Chemistry C* **126**, 6925 (2022).

[8] I. N. Levine, D. H. Busch, and H. Shull, *Quantum chemistry*, Vol. 6 (Pearson Prentice Hall Upper Saddle River, NJ, 2009).

[9] R. M. Martin, L. Reining, and D. M. Ceperley, *Interacting Electrons: Theory and Computational Approaches* (Cambridge University Press, 2016).

[10] A. Altland and B. D. Simons, *Condensed Matter Field Theory*, 2nd ed. (Cambridge University Press, 2010).

[11] R. M. Martin, *Electronic Structure: Basic Theory and Practical Methods* (Cambridge University Press, 2004).

[12] R. J. Bartlett and M. Musial, Coupled-cluster theory in quantum chemistry, *Reviews of Modern Physics* **79**, 291 (2007).

[13] V. I. Anisimov, I. V. Solovyev, M. A. Korotin, M. T. Czyzyk, and G. A. Sawatzky, Density-functional theory and nio photoemission spectra, *Phys. Rev. B* **48**, 16929 (1993).

[14] M. Cococcioni and S. de Gironcoli, Linear response approach to the calculation of the effective interaction parameters in the LDA + U method, *Phys. Rev. B* **71**, 035105 (2005).

[15] V. L. Campo and M. Cococcioni, Extended dft + u + v method with on-site and inter-site electronic interactions, *Journal of Physics: Condensed Matter* **22**, 055602 (2010).

[16] J. Huang, S.-H. Lee, Y.-W. Son, A. Supka, and S. Liu, First-principles study of two-dimensional ferroelectrics using self-consistent hubbard parameters, *Phys. Rev. B* **102**, 165157 (2020).

[17] N. Tancogne-Dejean and A. Rubio, Parameter-free hybridlike functional based on an extended hubbard model: DFT + u + v, *Phys. Rev. B* **102**, 155117 (2020).

[18] M. Cococcioni and N. Marzari, Energetics and cathode voltages of Limpo₄ olivines ($m = \text{Fe, mn}$) from extended hubbard functionals, *Phys. Rev. Mater.* **3**, 033801 (2019).

[19] C. Ricca, I. Timrov, M. Cococcioni, N. Marzari, and U. Aschauer, Self-consistent DFT + u + v study of oxygen vacancies in srtio₃, *Phys. Rev. Res.* **2**, 023313 (2020).

[20] R. Mahajan, I. Timrov, N. Marzari, and A. Kashyap, Importance of intersite hubbard interactions in β -mno₂: A first-principles DFT + u + v study, *Phys. Rev. Mater.* **5**, 104402 (2021).

[21] J. Yang, T. Zhu, and S. Liu, Onsite and intersite electronic correlations in the hubbard model for halide perovskites, *Phys. Rev. B* **106**, 195159 (2022).

[22] I. Timrov, F. Aquilante, M. Cococcioni, and N. Marzari, Accurate electronic properties and intercalation voltages of olivine-type li-ion cathode materials from extended hubbard functionals, *PRX Energy* **1**, 033003 (2022).

[23] B. G. Jang, M. Kim, S.-H. Lee, W. Yang, S.-H. Jhi, and Y.-W. Son, Intersite coulomb interactions in charge-ordered systems, *Phys. Rev. Lett.* **130**, 136401 (2023).

[24] P. Giannozzi, O. Andreussi, T. Brumme, O. Buna, M. B. Nardelli, M. Calandra, R. Car, C. Cavazzoni, D. Ceresoli, M. Cococcioni, N. Colonna, I. Carnimeo, A. D. Corso, S. de Gironcoli, P. Delugas, R. A. DiStasio, A. Ferretti, A. Floris, G. Fratesi, G. Fugallo, R. Gebauer, U. Gerstmann, F. Giustino, T. Gorni, J. Jia, M. Kawamura, H.-Y. Ko, A. Kokalj, E. Küçükbenli, M. Lazzeri, M. Marsili, N. Marzari, F. Mauri, N. L. Nguyen, H.-V. Nguyen, A. O. de-la Roza, L. Paulatto, S. Poncé, D. Rocca, R. Sabatini, B. Santra, M. Schlipf, A. P. Seitsonen, A. Smogunov, I. Timrov, T. Thonhauser, P. Umari, N. Vast, X. Wu, and S. Baroni, Advanced capabilities for materials modelling with quantum espresso, *Journal of Physics: Condensed Matter* **29**, 465901 (2017).

[25] J. Heyd, G. E. Scuseria, and M. Ernzerhof, Hybrid functionals based on a screened Coulomb potential, *The Journal of Chemical Physics* **118**, 8207 (2003).

[26] L. Lin, Adaptively compressed exchange operator, *Journal of Chemical Theory and Computation* **12**, 2242 (2016).

[27] I. Timrov, N. Marzari, and M. Cococcioni, Hp – a code for the calculation of hubbard parameters using density-functional perturbation theory, *Computer Physics Communications* **279**, 108455 (2022).

[28] H. T. Stokes and D. M. Hatch, FINDSYM: program for identifying the space-group symmetry of a crystal, *Journal of Applied Crystallography* **38**, 237 (2005).

[29] C. Bradley and A. Cracknell, *The mathematical theory of symmetry in solids: representation theory for point groups and space groups* (Oxford University Press, 2010).

[30] L. Elcoro, B. Bradlyn, Z. Wang, M. G. Vergniory, J. Cano, C. Felser, B. A. Bernevig, D. Orobengoa, G. de la Flor, and M. I. Aroyo, Double crystallographic groups and their representations on the Bilbao Crystallographic Server, *Journal of Applied Crystallography* **50**, 1457 (2017).

[31] D. I. Khomskii, *Transition Metal Compounds* (Cambridge University Press, 2014).

- [32] F. Wrobel, H. Park, C. Sohn, H.-W. Hsiao, J.-M. Zuo, H. Shin, H. N. Lee, P. Ganesh, A. Benali, P. R. C. Kent, O. Heinonen, and A. Bhattacharya, Doped nio: The mottness of a charge transfer insulator, *Phys. Rev. B* **101**, 195128 (2020).
- [33] M. Yu, S. Yang, C. Wu, and N. Marom, Machine learning the hubbard u parameter in dft+ u using bayesian optimization, *npj Computational Materials* **6**, 180 (2020).
- [34] H. J. Kulik, M. Cococcioni, D. A. Scherlis, and N. Marzari, Density functional theory in transition-metal chemistry: A self-consistent hubbard u approach, *Phys. Rev. Lett.* **97**, 103001 (2006).
- [35] I. Timrov, N. Marzari, and M. Cococcioni, Hubbard parameters from density-functional perturbation theory, *Phys. Rev. B* **98**, 085127 (2018).
- [36] A. E. Bocquet, T. Mizokawa, T. Saitoh, H. Namatame, and A. Fujimori, Electronic structure of 3d-transition-metal compounds by analysis of the 2p core-level photoemission spectra, *Phys. Rev. B* **46**, 3771 (1992).
- [37] L. Wang, T. Maxisch, and G. Ceder, Oxidation energies of transition metal oxides within the GGA+U framework, *Phys. Rev. B* **73**, 195107 (2006).
- [38] M. V. Mostovoy and D. I. Khomskii, Orbital ordering in charge transfer insulators, *Phys. Rev. Lett.* **92**, 167201 (2004).
- [39] J. Kuneš, V. I. Anisimov, S. L. Skornyakov, A. V. Lukyanov, and D. Vollhardt, Nio: Correlated band structure of a charge-transfer insulator, *Phys. Rev. Lett.* **99**, 156404 (2007).

Supplementary Material for “The role of Coulomb interaction on the electronic properties of monolayer NiX_2 ($\text{X} = \text{S, Se}$): A DFT+U+V study”

Sergio Bravo^{†1}, P.A. Orellana¹, and L. Rosales¹

[†]sergio.bravoc@usm.cl

Supplementary Tables

Material	Lattice constant	Ni-X distance	X-X distance	X-Ni-X angle	X vertical distance
NiSe_2 NM	3.540 Å	2.390 Å	3.211 Å	95.58°	1.238 Å
NiS_2 NM	3.306 Å	2.248 Å	3.047 Å	94.68°	1.188 Å
NiSe_2 LR	3.709 Å	2.484 Å	3.304 Å	96.61°	1.258 Å
NiS_2 LR	3.549 Å	2.361 Å	3.114 Å	97.47°	1.172 Å

Table S.1: Geometrical data for the NiX_2 materials obtained from the first-principles calculations. NM stands for the nonmagnetic phases presented in the main text, with and without Hubbard corrections. LR indicates the phase that arises from the linear response calculation without any further modification. X=(S,Se) as appropriate.

Supplementary Figures

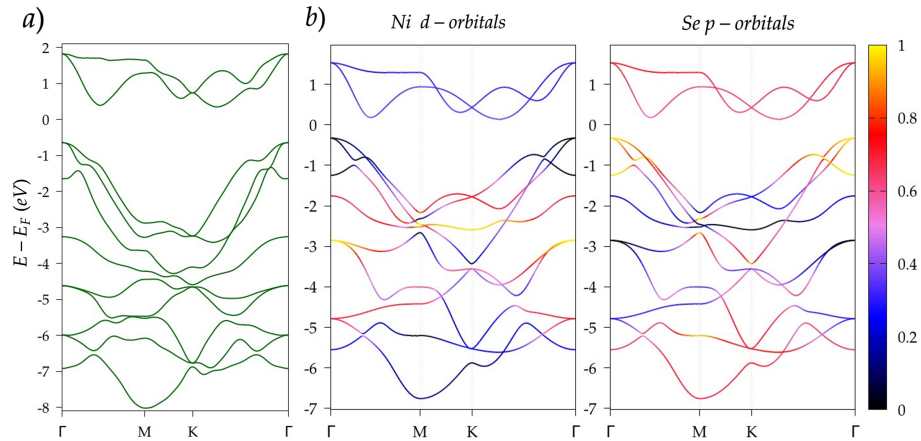


Figure S.1: a) HSE electronic band structure for NiS_2 . b) PBE electronic band structure with orbital projections for (left) Ni d-orbitals and (right) S p-orbitals. The color scale at the right is in $(\text{states} \cdot \text{\AA}^2)/\text{eV}$ units.

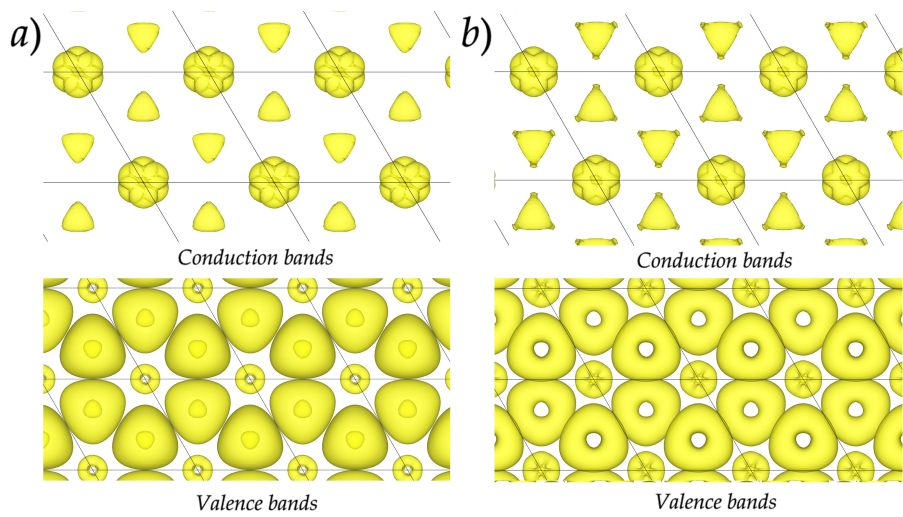


Figure S.2: a) Integrated local density of states for (top panel) lowest conduction bands and (bottom panel) top of the valence bands with the HSE functional NiS₂. b) Integrated local density of states for (top panel) lowest conduction bands and (bottom panel) top of the valence bands with the PBE functional NiS₂. In both cases, the valence band range is 0.4 eV from the top of the bands.

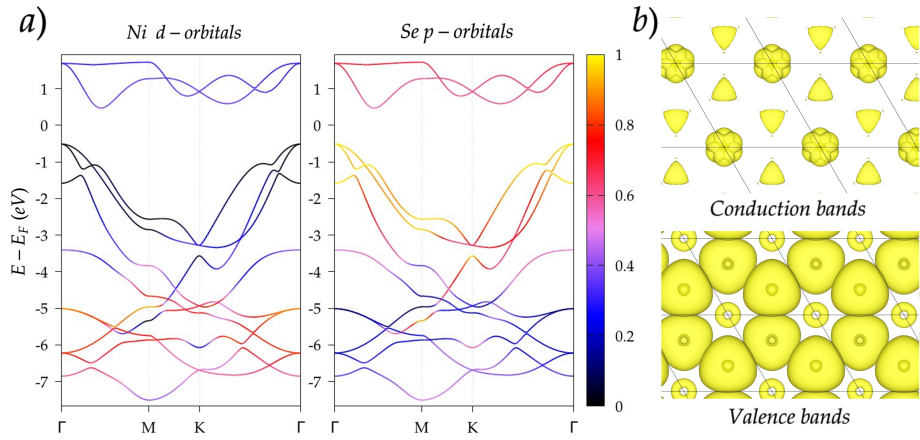


Figure S.3: a) Orbital-projected Electronic band structure at the DFT+U+V level of NiS_2 with parameters from linear response with modified $V_{\text{Ni}-\text{S}}$ parameter. The color scale at the right is in $(\text{states} \cdot \text{\AA}^2)/\text{eV}$ units. b) Integrated local density of states for (top panel) lowest conduction bands and (bottom panel) top of the valence bands using the DFT-UV functional with linear response parameters with modified $V_{\text{Ni}-\text{S}}$.

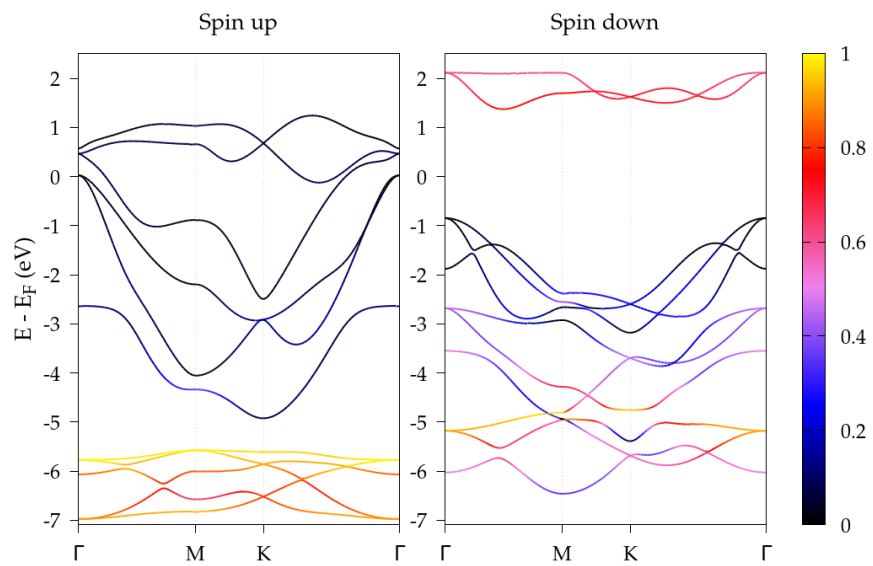


Figure S.4: a) Spin-polarized orbital-projected Electronic band structure at the DFT+U+V level of Ni d orbitals for NiSe_2 with parameters from linear response calculation as presented in the main text. The color scale at the right is in (states $\cdot \text{\AA}^2$)/eV units.

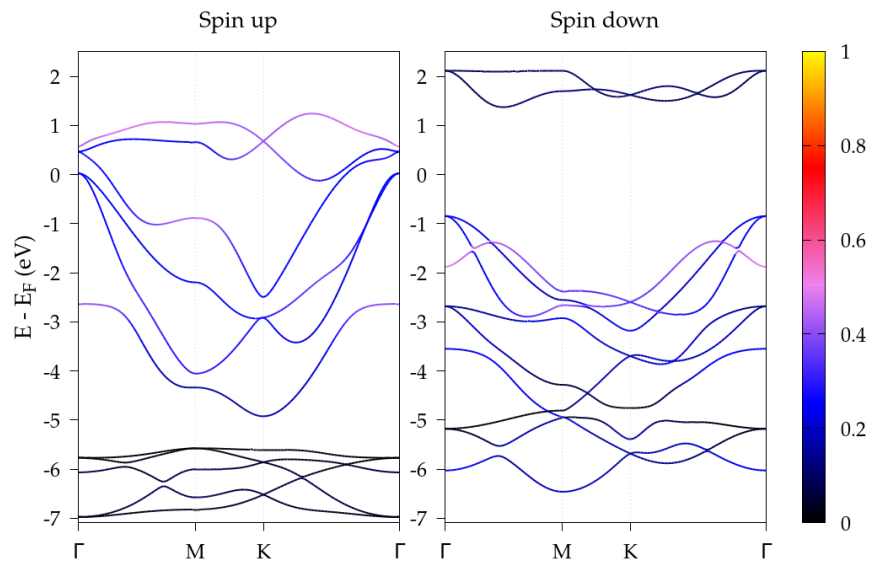


Figure S.5: a) Spin-polarized orbital-projected Electronic band structure at the DFT+U+V level of Se p orbitals for NiSe_2 with parameters from linear response calculation as presented in the main text. The color scale at the right is in (states $\cdot \text{\AA}^2$)/eV units.

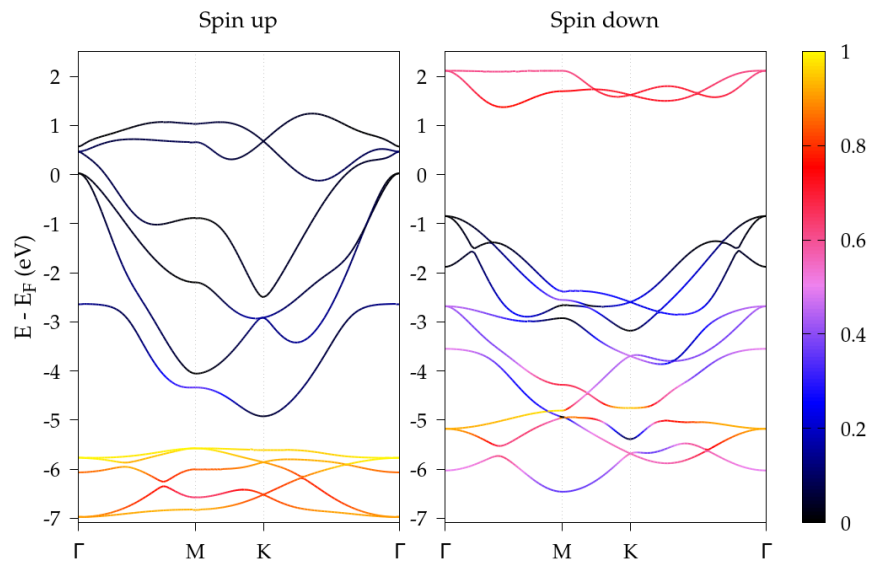


Figure S.6: a) Spin-polarized orbital-projected Electronic band structure at the DFT+U+V level of Ni d orbitals for NiS_2 with parameters from linear response calculation as presented in the main text. The color scale at the right is in $(\text{states} \cdot \text{\AA}^2)/\text{eV}$ units.

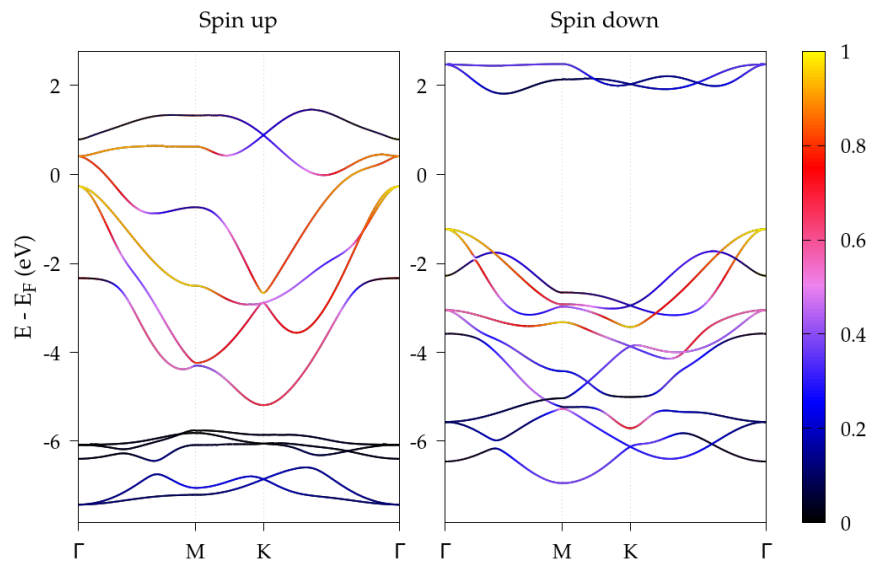


Figure S.7: a) Spin-polarized orbital-projected Electronic band structure at the DFT+U+V level of S *p* orbitals for NiS₂ with parameters from linear response calculation as presented in the main text. The color scale at the right is in (states · Å²)/eV units.